

Crystal Growth of $\text{Ag}_3\text{MO}_x\text{F}_{6-x}$ ($M = \text{V}$, $x = 2$; $M = \text{Mo}$, $x = 3$)Julia M. Chamberlain, Thomas A. Albrecht, Julien Lesage, Frédéric Sauvage,
Charlotte L. Stern, and Kenneth R. Poeppelmeier*

Department of Chemistry, Northwestern University, Evanston, Illinois 60208-3113

Received July 5, 2010; Revised Manuscript Received August 30, 2010

© This paper contains enhanced objects available on the Internet at <http://pubs.acs.org/crystal>.

ABSTRACT: Understanding the complex relationship between synthesis conditions, in particular temperature and composition, led to single crystals of the cryolite type phases $\text{Ag}_3\text{MoO}_3\text{F}_3$ and $\text{Ag}_3\text{VO}_2\text{F}_4$. These crystals form in a reversible thermodynamic process from dissolved species when the solution is heated. Single crystal structural data reveal the Mo^{6+} cation distorted toward facially coordinated oxides for $\text{Ag}_3\text{MoO}_3\text{F}_3$, and the V^{5+} cation toward the edge of the cis-oxide positions for $\text{Ag}_3\text{VO}_2\text{F}_4$. Local ordering of oxide and fluoride ligands is observed for both structures.

Introduction

Inorganic silver transition metal oxide fluorides enable new cathode technology in medical device batteries, such as those used for implantable cardioverter defibrillators.¹ Silver vanadium oxide fluoride, $\text{Ag}_4\text{V}_2\text{O}_6\text{F}_2$ (SVOF),² has been shown to have superior electrochemical properties for this application and shows great promise, especially when synthesized at lower temperatures.³ Silver transition metal oxide fluoride materials have been prepared using a variety of synthetic approaches, including traditional solid state methods⁴ and mechanochemical reactions.^{5,6} This work examines the process of synthesizing such materials using soft chemistry solution synthesis techniques at low temperatures (room temperature to 150 °C) using an aqueous hydrofluoric acid mineralizer.

Recent work reveals that SVOF^{2,7} offers greater capacity and higher open circuit voltage owing to the higher silver density as well as increased electronegativity of fluoride, respectively, resulting in improved electrochemical performance. Molybdenum oxide fluoride phases with high silver density such as $\text{Ag}_6\text{Mo}_2\text{O}_7\text{F}_3\text{Cl}$ (SMOFC)^{8–10} and $\text{Ag}_3\text{MoO}_3\text{F}_3$ (SMOF)⁵ have received recent attention for electrochemical applications. Various materials of the formula $A_3\text{MO}_x\text{F}_{6-x}$ ($A = \text{Ag}^+$; $M = \text{Ti}^{4+}$, $x = 1$; $M = \text{V}^{5+}$, Nb^{5+} , $x = 2$; $M = \text{Mo}^{6+}$, W^{6+} , $x = 3$) adopt the cryolite structure type^{3–6} and are of interest as cathode materials owing to high silver content and increased electronegativity. This study explores the $\text{Ag}_2\text{O}-\text{MoO}_3-\text{HF}_{(\text{aq})}$ and $\text{Ag}_2\text{O}-\text{V}_2\text{O}_5-\text{HF}_{(\text{aq})}$ systems from room temperature to 150 °C and introduces hydrothermally synthesized $\text{Ag}_3\text{MoO}_3\text{F}_3$ and $\text{Ag}_3\text{VO}_2\text{F}_4$, two recently reported compounds,^{3,5} to a growing family of oxyfluoride materials with a potential value for use as cathodes for primary lithium batteries.

Experimental Section

Caution. Hydrofluoric acid is toxic and corrosive and must be handled with extreme caution and the appropriate protective gear! If contact with the liquid or vapor occurs, proper treatment procedures should be followed immediately.^{11–13}

Materials. Ag_2O (99+ Fisher), MoO_3 (99.95% Alfa-Aesar), V_2O_5 (99.6% Alfa-Aesar), and aqueous hydrofluoric acid (48–50% HF by weight, Fisher) were used as received.

Synthesis. Polycrystalline $\text{Ag}_3\text{MoO}_3\text{F}_3$ was prepared from a reaction of 0.4811 g (2.076×10^{-3} mol) of Ag_2O , 0.1706 g (1.185×10^{-3} mol) of MoO_3 , and 0.2288 g of $\text{HF}_{(\text{aq})}$ (5.603×10^{-3} mol HF) in a heat-sealed FEP Teflon pouch.¹⁴ The pouch was placed in a 125 mL poly(tetrafluoroethylene) (PTFE) Teflon-lined Parr autoclave, backfilled with 42 mL of deionized H_2O . Up to seven pouches of varied compositions can be simultaneously placed in the autoclave to ensure identical reaction conditions and to complete a greater number of reactions at a time.¹⁵ The autoclave was heated at 150 °C for 24 h and cooled at a rate of 6 °C/h. The pouch was opened in air, and the contents were vacuum-filtered to recover beige polycrystalline $\text{Ag}_3\text{MoO}_3\text{F}_3$.

Identical reaction conditions with different reagent quantities were used to synthesize Ag_2MoO_4 , $\text{Ag}_2\text{Mo}_2\text{O}_7$, and an unknown phase. Products were characterized by powder X-ray diffraction.

Ag_2MoO_4 was made using 0.3472 g (1.498×10^{-3} mol) of Ag_2O , 0.2159 g (1.500×10^{-3} mol) of MoO_3 , and 0.2378 g of $\text{HF}_{(\text{aq})}$ (5.705×10^{-3} mol HF).

$\text{Ag}_2\text{Mo}_2\text{O}_7$ was made using 0.4848 g (2.092×10^{-3} mol) of Ag_2O , 0.6024 g (4.185×10^{-3} mol) of MoO_3 , and 0.1714 g of $\text{HF}_{(\text{aq})}$ (4.198×10^{-3} mol HF). The end-product recovered from the pouch consisted of yellow needles of $\text{Ag}_2\text{Mo}_2\text{O}_7$ with Ag_2MoO_4 as a secondary polycrystalline phase.

A new silver molybdenum phase of unknown structure was made using 0.1737 g (7.496×10^{-4} mol) of Ag_2O , 0.2159 g (1.499×10^{-3} mol) of MoO_3 , and 0.2688 g of $\text{HF}_{(\text{aq})}$ (6.451×10^{-3} mol HF).

Single crystals of $\text{Ag}_3\text{MoO}_3\text{F}_3$ were prepared from a reaction of 0.2108 g (9.097×10^{-4} mol) of Ag_2O , 0.0652 g (4.530×10^{-4} mol) of MoO_3 , and 0.2794 g of $\text{HF}_{(\text{aq})}$ (6.843×10^{-3} mol HF). This differs from the above polycrystalline synthesis for $\text{Ag}_3\text{MoO}_3\text{F}_3$ in that the reagent ratio consists of approximately 15% more moles of Ag and more than three times the moles of HF, with respect to Mo. After the described hydrothermal reaction cycle, all of the starting materials had dissolved in solution. A small (unrecoverable) quantity of beige-colored powder (similar in appearance to polycrystalline $\text{Ag}_3\text{MoO}_3\text{F}_3$, described above) was visible in the pouch. The pouch was placed into a water bath at room temperature and gradually heated to boiling over a 30–60 min period. After remaining in the water bath at 100 °C for 1–4 h, yellow crystals were visible in the pouch. The pouch was removed from the bath, opened, and its contents were immediately vacuum filtered to recover yellow crystals of $\text{Ag}_3\text{MoO}_3\text{F}_3$ with an average size ranging from 0.2–0.3 mm. Owing to the presence of small amounts of Ag_2MoO_4 , the approximate yield of $\text{Ag}_3\text{MoO}_3\text{F}_3$ obtained by this method is 16% based on MoO_3 (12% based on Ag_2O). Ag_2O is the more soluble of the reagents in $\text{HF}_{(\text{aq})}$, and thus an excess was required.

Pouches that were returned to room temperature prior to opening showed complete dissolution of the yellow crystals in the aqueous HF solution. This process is reversible and repeatable for sealed pouches over multiple heating and cooling cycles in the

*To whom correspondence should be addressed. E-mail: krp@northwestern.edu.

boiling water bath. Crystals may also be synthesized directly from reagents dissolved in HF_(aq) at room temperature and heated in the sealed pouch at 100 °C for between 1 and 4 h, thus circumventing the hydrothermal step.

While the Ag₂O–V₂O₅–HF_(aq) system under hydrothermal conditions is reported elsewhere,⁷ alternate conditions have yielded a new silver oxide fluoride, Ag₃VO₂F₄.³ This new phase was initially synthesized from a reaction of 0.3977 g (1.716 × 10⁻³ mol) of Ag₂O, 0.0779 g (4.28 × 10⁻⁴ mol) of V₂O₅, and 0.2555 g of HF_(aq) (6.257 × 10⁻³ mol HF) in a FEP Teflon pouch. The pouch was sealed and agitated by hand to mix the reagents at room temperature until a uniform red powder was obtained within a yellow solution. The pouch was opened in air and the contents were vacuum filtered to retrieve bright red polycrystalline Ag₃VO₂F₄.

Single crystals of Ag₃VO₂F₄ were crystallized from a solution containing 0.3975 g (1.715 × 10⁻³ mol) of Ag₂O, 0.0777 g (4.27 × 10⁻⁴ mol) of V₂O₅, and 0.5504 g of HF_(aq) (1.348 × 10⁻² mol HF) in a heat sealed FEP Teflon pouch. The reagents in the pouch were mixed well at room temperature until the silver oxide and vanadium oxide dissolved to give a yellow solution. This synthesis allowed the complete dissolution of the reactants as well as any products at room temperature, owing to the presence of approximately twice the amount of HF_(aq) as the polycrystalline synthesis above. The pouch was placed into a water bath at room temperature which was slowly heated to a boil over 3–4 h. After heating at 100 °C for 30 min, the pouch was quickly removed from the bath, opened, and its contents were filtered to recover many crystals of Ag₃VO₂F₄, with an average size range of 0.3–0.4 mm.

Crystals of Ag₃MoO₃F₃ (yellow) and Ag₃VO₂F₄ (red) from the boiling water bath synthesis were selected for single crystal X-ray diffraction studies.

Crystallographic Determination. Single crystals were handled in Infineum oil for all manipulation and data were collected at low-temperature to prevent decomposition of the structure during measurement. Crystals used for structural determination were selected under a polarized microscope, and no evidence of physical twin domains was observed.

One single-crystal platelet of Ag₃MoO₃F₃ of approximate dimensions 0.07 × 0.07 × 0.02 mm³ was examined. X-ray diffraction data were collected at 153 K with Mo-Kα radiation on a BRUKER AXS SMART-1000 CCD diffractometer, integrated with the SAINT-PLUS program suite, corrected for absorption with XPREP (Gaussian face-indexed method) and further scaled by SADABS.¹⁶

Several crystals of Ag₃VO₂F₄ were examined and all showed signs of twinning. We report here the results from a crystal platelet that gave the best refinement, with approximate dimensions 0.11 × 0.22 × 0.27 mm³. X-ray diffraction data were collected at 100 K with Mo-Kα radiation on a BRUKER AXS Kappa Apex II CCD diffractometer, integrated with the Apex II program suite.¹⁶ A multiscan absorption correction was applied via TWINABS.¹⁷

Powder X-ray Diffraction. Powder X-ray diffraction patterns were collected at room temperature on a Rigaku XDS 2000 with Ni-filtered Cu Kα radiation (λ = 1.5418 Å) and compared against patterns in the Joint Committee of Powder Diffraction Standards (JCPDS) database. Sample preparation and measurement were performed so as to minimize hydrolysis of the compound by moisture in air.

Electrochemical Measurements. The lithium insertion properties of Ag₃MoO₃F₃ and Ag₃VO₂F₄ were investigated using a two-electrode Swagelok-type cell with a lithium metal foil used as a reference and counter electrode. Two pieces of Whatman GF/D borosilicate glass fiber sheet separator were thoroughly soaked with 1 M LiPF₆ EC/DMC 1:1 electrolyte (named LP30 - Merck Selectipur grade). The cathode material was composed of single crystals mixed with 13% SP-type carbon black and ground using a mortar and pestle in an Ar-filled glovebox to prevent hydrolysis. The electrochemical properties of the cathode were monitored by a VMP multipotentiostat (Biologic SA, Claix, France).

Results and Discussion

Products. Products of the Ag₂O–MoO₃–HF_(aq) reaction system at 150 °C (Figure 1) include both silver molybdenum oxide and oxide-fluoride compounds. Owing to the differing solubility of Ag₂O and MoO₃ in aqueous hydrofluoric acid,

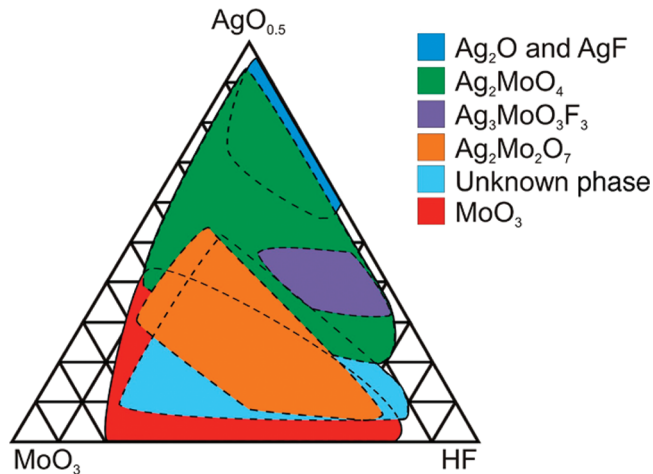


Figure 1. The composition space diagram for the Ag₂O–MoO₃–HF_(aq) system shows regions where oxide and oxide fluoride products form at 150 °C. Ag–Mo products were observed in the green, purple, and orange regions; starting materials were observed in the blue and red areas; and a phase of unknown structure is shown in light blue. The presence of multiple phases is shown as overlapping zones, denoted by dotted lines. 96 reactions were conducted to survey the composition space.

products are not necessarily stoichiometric compared to the molar ratios of the starting materials used, an effect that is more pronounced at higher HF ratios.¹⁸ For example, the two silver molybdenum oxide products, Ag₂MoO₄ and Ag₂Mo₂O₇,¹⁹ result from approximate corresponding mole ratios of silver and molybdenum in the starting materials (2:1:*x* and 1:1:*x*, respectively, for Ag/Mo/HF with *x* ≤ 4). At these ratios, the aqueous HF acts primarily as a mineralizer and solvent for the reaction. However, in the conditions used to synthesize polycrystalline Ag₃MoO₃F₃, the molar ratio of Ag/Mo/HF was 3.5:1:4.7, representing an increase in the respective molar quantities of both Ag and HF. In the synthesis of single crystals, the Ag/Mo/HF ratio increased to 4:1:15, demonstrating the more soluble nature of Ag₂O compared to MoO₃ in aqueous HF, and the necessity of higher HF ratios for its role to extend to that of a reagent as well as a mineralizer.

At high metal oxide mole fractions, starting materials do not fully dissolve in the aqueous HF, and Ag₂O and MoO₃ are observed as the primary phases after the hydrothermal heating cycle. At high HF mole fractions, starting materials remain in solution, and solid products are either absent, or recovered in quantities too small for powder diffraction. In the areas of the diagram where product yields allow characterization by powder X-ray diffraction (XRD), multiple phases are often observed in a single pouch, indicated in the composition space diagram by overlapping areas between regions. Microcrystalline powders (<0.01 mm) were observed for all products except for Ag₂Mo₂O₇, which formed yellow rectangular plate crystals under the 24 h hydrothermal cycle at 150 °C.^{20,21}

A secondary phase of unknown structure was observed in a reaction with a Ag/Mo/HF starting material molar ratio of 1:1:4.3. This phase appears as a tan-colored powder and exhibits an XRD pattern identical to the unidentified phase reported by Tong et al.⁵ Further characterization will be reported elsewhere.

Hydrolysis. Under hydrothermal conditions at 150 °C, the Teflon pouch reaction vessels become semipermeable to the

water backfill in the pressure vessel, allowing water to enter the pouch and participate in the reaction. The amount of water that enters the pouch influences the concentration of HF, the solubility of the reagents, and the reaction products. At temperatures lower than 150 °C, the Teflon is less permeable, and at temperatures of 100 °C and lower, such as the boiling water bath, water does not permeate the pouch. Therefore, products that hydrolyze should be formed at temperatures lower than those that allow water to diffuse into the reaction pouch. This behavior allows the exploration of products that may hydrolyze using the hydrothermal reaction technique at temperatures above 100 °C. For example, in the previously reported synthesis of $\text{Ag}_4\text{V}_2\text{O}_6\text{F}_2$ (SVOF),³ polycrystalline $\text{Ag}_3\text{VO}_2\text{F}_4$ was observed to react with water at room temperature to yield polycrystalline SVOF (eq 1).



When more water is present, as in the case of lower aqueous HF concentrations, SVOF is the observed product owing to this hydrolysis reaction. Likewise, the water that enters the Teflon pouch during hydrothermal synthesis at 150 °C hydrolyzes any $\text{Ag}_3\text{VO}_2\text{F}_4$ present to SVOF. This relationship is an important concept in the preparation of small particles for improved electrochemical performance.³ Under hydrothermal conditions at 200 °C, a second hydrolysis reaction (eq 2) is observed, whereby the oxide fluoride is fully hydrolyzed to the corresponding oxide species.



$\text{Ag}_3\text{MoO}_3\text{F}_3$ shows a different hydrolysis relationship (eq 3), observed as a reaction with ambient water in the atmosphere.



This hydrolysis relationship is one of several equilibria within the Teflon pouch, and the uptake of water through the pouch membrane is a likely contributor to the presence of Ag_2MoO_4 throughout the composition space at 150 °C. When reacted with an excess of water, $\text{Ag}_3\text{MoO}_3\text{F}_3$ decomposes entirely and shows no intermediate oxide fluoride compound between the $\text{Ag}_3\text{MO}_x\text{F}_{6-x}$ and the purely oxide phase, such as SVOF in the silver vanadium system.

Synthesis. Alternative synthetic procedures for $\text{Ag}_3\text{MoO}_3\text{F}_3$ and $\text{Ag}_3\text{VO}_2\text{F}_4$ recently were reported;^{3,5} here, they are synthesized in single crystal form from reaction conditions that involved precipitation upon heating (Figure 2). This crystal growth technique uses both hydrothermal and solution chemistry to precipitate (or in this case crystallize) a product from dissolved species in solution. $\text{Ag}_3\text{MoO}_3\text{F}_3$ and $\text{Ag}_3\text{VO}_2\text{F}_4$ demonstrate a negative temperature coefficient of solubility, whereby they become less soluble as temperature increases. While a negative temperature coefficient of solubility is observed for various compounds,^{22–25} it is unusual by comparison to traditional solubility trends. We hypothesize that two nonexclusive phenomena contribute to this outcome: (1) a temperature increase may affect solution acidity, causing reactive species in solution to adjust according to the consequential influx or removal of H^+ , and (2) that temperature may affect the coordinating species in solution such as waters of hydration and associated HF molecules, contributing to an entropically driven process. The overarching explanation for

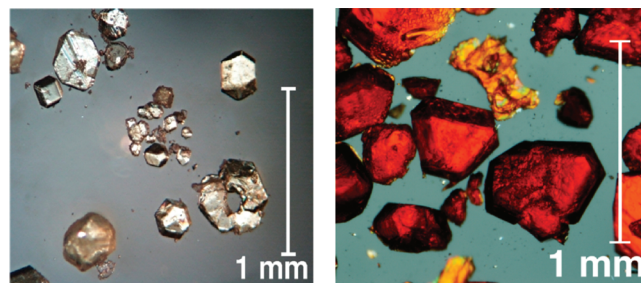


Figure 2. Single crystals of $\text{Ag}_3\text{MoO}_3\text{F}_3$ (left) and $\text{Ag}_3\text{VO}_2\text{F}_4$ (right) synthesized by precipitation upon heating.

both hypotheses is thermodynamic effects of entropy and enthalpy.

The primary advantage of this crystal growth technique is its completion in a closed, transparent vessel, facilitating the careful control of reagent concentrations and stoichiometries while the reaction proceeds. Crystal growth is visible with the naked eye, and the heating profile can be lengthened to accommodate slower crystal growth (a video of $\text{Ag}_3\text{VO}_2\text{F}_4$ crystal growth (at 90× speed) in a boiling water bath is available in AVI format in the HTML version of this article). An additional advantage is the safe containment of the hydrofluoric acid reagent in the vessel during the reaction process. The lower temperature method of boiling the pouch at 100 °C (without the hydrothermal pressure vessel) prevents the addition of water to the reaction vessel through the membrane. As a result, different products can be formed at this temperature, and better control and reproducibility of precise mole ratios may be achieved with aqueous HF concentrations as high as 48%. This method also accesses the single crystal products that form at these higher HF concentrations at 100 °C, which are not always achieved using standard hydrothermal or high temperature solid-state methods. The single crystalline products allow examination of local order and out-of-center distortions in the anionic units in these two recently reported cryolite type compounds.

Crystal Structures. $\text{Ag}_3\text{MoO}_3\text{F}_3$. Heavy atoms in the structure of $\text{Ag}_3\text{MoO}_3\text{F}_3$ were located via direct methods with SHELXS.²⁶ The remaining positions were determined by successive difference Fourier analysis. The structure was refined with SHELXL against F^2 by full matrix least-squares techniques, and all refinements included anisotropic displacement parameters and further correction from secondary extinction effects.

The initial model led to $R = 0.0632$ and $wR_2 = 0.1999$ values. Given the space group $P2_1/n$, two atoms (Ag2, Wyckoff position $2b$ and Mo, Wyckoff position $2a$) are located in special positions, while the remaining Ag1 atom and the three remaining maxima lay in general positions. As a result, considering the highest 6+ oxidation state for molybdenum (expected by the highly oxidative condition of synthesis), the composition $\text{Ag}_3\text{MoO}_3\text{F}_3$ is proposed with $Z = 2$. The three positions around Mo must therefore be statistically occupied by oxygen and fluorine atoms with an overall 0.5 O/F ratio. Equivalent Mo–O/F distances of about 1.906 Å are observed, leading to a fully disordered model with poor chemical description. Moreover, an important electronic density residue of $4.33 \text{ e}^- \text{ \AA}^{-3}$ is visible at 0.47 Å of the Mo atomic position. The Mo position was thus allowed to move out of its center of symmetry with fixed half occupancy (0.5) to conserve the stoichiometry of the compound. Two groups of Mo–X distances can now be clearly distinguished: three

Table 1. Crystallographic Data for $\text{Ag}_3\text{MoO}_3\text{F}_3$ and $\text{Ag}_3\text{VO}_2\text{F}_4$ Single Crystals

formula	$\text{Ag}_3\text{MoO}_3\text{F}_3$	$\text{Ag}_3\text{VO}_2\text{F}_4$
formula weight (g/mol^{-1})	524.55	482.55
space group	$P2_1/n$ (No. 14)	$P2_1/n$ (No. 14)
a (\AA)	5.8050(6)	5.7568(2)
b (\AA)	5.886(6)	5.7811(2)
c (\AA)	8.295(8)	8.0883(3)
β (deg)	90.45(1)	90.6610(15)
V (\AA^3)	285.6(5)	269.166(17)
Z	2	2
T (K)	153(2)	98(2)
λ (\AA)	0.71073	0.71073
ρ_{calc} (g/cm^3)	6.100	5.954
μ (mm^{-1})	12.277	12.447
$R(F)^a$	0.0297	0.0393
$wR_2(F^2)^b$	0.0803	0.1159

$$^a R = \frac{\sum ||F_o| - |F_c||}{\sum |F_o|}, \quad ^b wR_2 = \frac{[\sum w(F_o^2 - F_c^2)^2]}{[\sum w(F_o^2)^2]}^{1/2}.$$

short Mo–O distances (1.795(3), 1.773(3), and 1.734(3) \AA) and three long Mo–F distances (2.076(3), 2.076(3), and 2.093(3) \AA), as observed in the already existing ordered oxifluorides.^{8,27} Each of the three ligand sites are statistically occupied by 0.5 oxygen and 0.5 fluorine atoms with their atomic parameters (atomic coordinates and anisotropic atomic displacement parameters) being constrained to the same values. The final refinement based on this model gives significantly lower values for $R = 0.0297$ and $wR_2 = 0.0803$, without any substantial electron density elsewhere. Structural data are reported in Table 1.

The crystal studied showed modulated q -vectors ($\bar{q}1 = 0.5082(5)\bar{a}^* + 0.2416(5)\bar{b}^* + 0.2389(7)\bar{c}^*$ and $\bar{q}2 = 0.5080(5)\bar{a}^* - 0.2411(5)\bar{b}^* + 0.2397(7)\bar{c}^*$, close to commensurability), observed as satellite reflections of very low intensities. See SI Figure 1 in the Supporting Information for a precession figure. Owing to crystal quality, in particular its high mosaicity (correlated to the elongated shape of the main reflections), no attempts have been made to solve the modulated structure, as the refined average model gives satisfactory results.

$\text{Ag}_3\text{VO}_2\text{F}_4$. The diffraction pattern of the $\text{Ag}_3\text{VO}_2\text{F}_4$ single crystal shows evidence of pseudomerohedral twinning. The predominance of one component helped to determine the basic unit cell, and twin laws for five additional components were found with the program CELL_NOW.²⁸ (See CIF, Supporting Information.) The proposed unit cell parameters for $\text{Ag}_3\text{VO}_2\text{F}_4$ appeared to be close to the cell parameters of the isostructural $\text{Ag}_3\text{MoO}_3\text{F}_3$. Nonmerohedral reflections were found in the $\text{Ag}_3\text{VO}_2\text{F}_4$ crystal, consistent with a 6-fold rotation around the same zone axis.

The structure of $\text{Ag}_3\text{VO}_2\text{F}_4$ was solved by direct methods using SHELXS with a “detwinned” reflection file prepared by TWINABS¹⁷ from the intensities of the first domain (HKL 4 option) of the second crystal. As expected, the same space group and basic structure as $\text{Ag}_3\text{MoO}_3\text{F}_3$ is observed, with an initial model leading to $R = 0.0927$, $wR_2 = 0.3123$, one group of six V–O/F distances (mean value of 1.853 \AA) and a first residue of $9.89 \text{ e}^- \text{\AA}^{-3}$ at 0.35 \AA of the V site. The vanadium atom was then allowed to move away from its center of symmetry with a fixed occupation ratio of 0.5. The analysis of the V–O/F distances clearly shows three groups of V–O/F distances. In the first, two short distances of 1.706(2) and 1.676(2) \AA , and in the second, two long distances of 2.003(2) and 2.025(2) \AA are calculated depending on which V atom is bonded to the ligands. Those four ligands sites O1/F1 and O2/F2 are therefore statistically

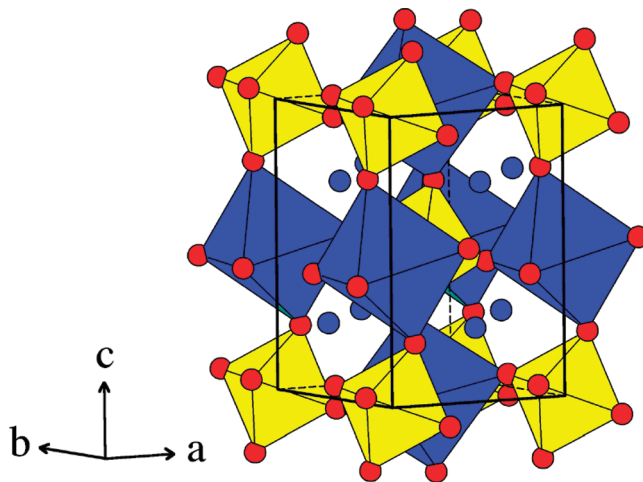


Figure 3. The $\text{Ag}_3\text{MoO}_3\text{F}_3$ unit cell showing discrete $[\text{MoO}_3\text{F}_3]^{3-}$ octahedra (yellow) interspersed by two crystallographically distinct silver sites (blue spheres denote 10-coordinate silver, while 6-coordinate silver cations are shown as blue octahedra). Oxide and fluoride ligands in the anionic unit are disordered throughout the structure, shown in red. The $\text{Ag}_3\text{VO}_2\text{F}_4$ unit cell is isostructural, with slightly smaller lattice parameters owing to the smaller ionic radius of V^{5+} .

occupied by 0.5 oxygen atom and 0.5 fluorine atom, with their atomic parameters (atomic coordinates and anisotropic atomic displacement parameters) being constrained to the same values. The two remaining ligands correspond to fluorine F3 with intermediate bond distances (1.867(2) and 1.887(2) \AA) from both V positions. This model is consistent with both the chemistry and the composition of $\text{Ag}_3\text{VO}_2\text{F}_4$, and gives values of $R = 0.0754$ and $wR_2 = 0.2157$. Two residues of 6.31 and $6.06 \text{ e}^- \text{\AA}^{-3}$ were observed at 0.39 \AA and 0.49 \AA from Ag1, respectively, and then introduced in the model, the sum of the three sites being constrained to unity, leading to values of $R_1 = 0.0622$ and $wR_2 = 0.1825$. The final refinement with this model, using the HKLF 5 option for more accurate solution and the determination of the twin domain ratios, gives $R = 0.0393$ and $wR_2 = 0.1159$ with negligible residual electron density. The occupancies of the Ag1 sites are split according to the ratios 0.63(2):0.30(2):0.077(16) and the twin ratios from domain I to VI are $t_I = 0.515(3)$, $t_{II} = 0.0066(15)$, $t_{III} = 0.0146(5)$, $t_{IV} = 0.396(3)$, $t_V = 0.0142(5)$, $t_{VI} = 0.0536(18)$.

Description of Structures. $\text{Ag}_3\text{MoO}_3\text{F}_3$ and $\text{Ag}_3\text{VO}_2\text{F}_4$ adopt the cryolite structure type, similar to that of perovskite (formula ABO_3), which comprises tilted corner-shared alternating Ag and Mo/V octahedra (the B sites), with 10-coordinate Ag in the A sites, as in the formulas $(\text{Ag}_2)(\text{AgMo})(\text{O}_3\text{F}_3)$ and $(\text{Ag}_2)(\text{AgV})(\text{O}_2\text{F}_4)$ (Figure 3). The $[\text{MoO}_3\text{F}_3]^{3-}$ and $[\text{VO}_2\text{F}_4]^{3-}$ anionic units are discrete in each structure, sharing corner oxide and fluoride ligands with the octahedrally coordinated B site silver cations. These structure solutions show preferential ordering of the *fac*- $[\text{MoO}_3\text{F}_3]^{3-}$ and *cis*- $[\text{VO}_2\text{F}_4]^{3-}$ units within the structure (Figure 4), observed by the split occupancy of the Mo and V site in the anion, as opposed to random O and F placement. The out-of-center distortions observed in each structure support the proposed O/F ratio for each compound respectively.

Similar perovskite-type structures have been observed in related compounds with similar unit cell dimensions: $\text{Ag}_3\text{-TiOF}_5$, $\text{Ag}_3\text{NbO}_2\text{F}_4$, and $\text{Ag}_3\text{WO}_3\text{F}_3$ were synthesized in polycrystalline form via traditional solid state techniques,⁴

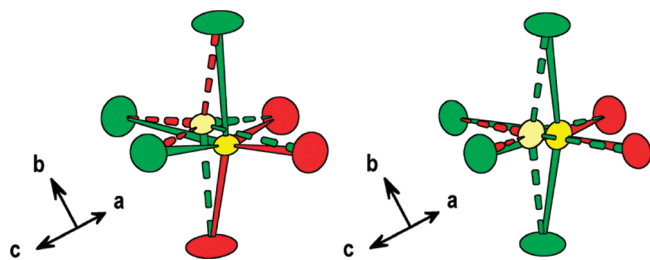


Figure 4. The $[\text{MoO}_3\text{F}_3]^{3-}$ anionic unit (left) shows an out-of-center distortion toward an octahedron face, resulting from preferential local ordering of oxide (red) and fluoride (green) atoms within the structure. The $[\text{VO}_2\text{F}_4]^{3-}$ anionic unit (right) shows a similar distortion toward the cis-oriented oxide edge of the octahedron.

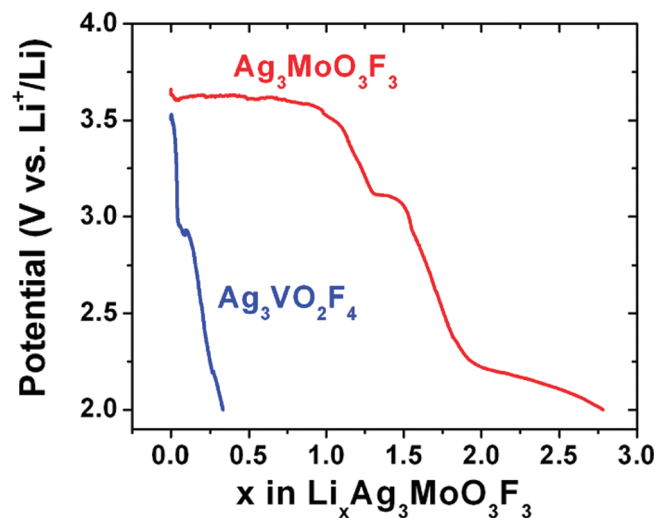


Figure 5. The electrochemical discharge curve of $\text{Ag}_3\text{MoO}_3\text{F}_3$ shows activity above 3 V, with silver reduction occurring at 3.55 V up to one lithium inserted. By comparison, the discharge curve for $\text{Ag}_3\text{VO}_2\text{F}_4$ shows lower activity, with insertion of only 0.3 Li^+ above 2 V.

however, oxide and fluoride ligand ordering is indiscernible in the polycrystalline study. A comparison of the silver molybdenum species to the sodium molybdenum structure reported by Brink et al. shows that the sodium cation successfully orders the oxide and fluoride ligands throughout the structure, observed in $\text{Na}_3\text{MoO}_3\text{F}_3$ (triclinic $P1$, metrically rhombohedral $R3$).²⁹ Although similar in size, the harder, less polarizable nature of the Na^+ cation imposes order in the extended structure,²⁷ whereas the more polarizable Ag^+ cation has greater flexibility in its coordination to the surrounding structure, resulting in only local ordering of O and F ligands.

Electrochemistry. The galvanostatic discharge of $\text{Ag}_3\text{MoO}_3\text{F}_3$ and $\text{Ag}_3\text{VO}_2\text{F}_4$ using a rate condition of D/10 (insertion of one lithium in 10 h) are shown in Figure 5. The silver reduction in $\text{Ag}_3\text{MoO}_3\text{F}_3$ takes place at a higher voltage ($E^\circ \text{Ag}^+/\text{Ag} = 3.55 \text{ V vs Li}^+/\text{Li}$) than in the benchmark cathode material $\text{Ag}_2\text{V}_4\text{O}_{11}$ ($E^\circ \text{Ag}^+/\text{Ag} = 3.25 \text{ V vs Li}^+/\text{Li}$)^{30,31} in agreement with our observation of other silver transition metal oxyfluoride compounds.^{2,10} This gain in potential results from the incorporation of fluoride within the silver environment, which reinforces the ionic character of the Ag–O/F bonds.

The galvanostatic curve for $\text{Ag}_3\text{MoO}_3\text{F}_3$ features three distinct regions of discharge. In the first, lithium reduces silver, seen as a plateau in the voltage curve corresponding to

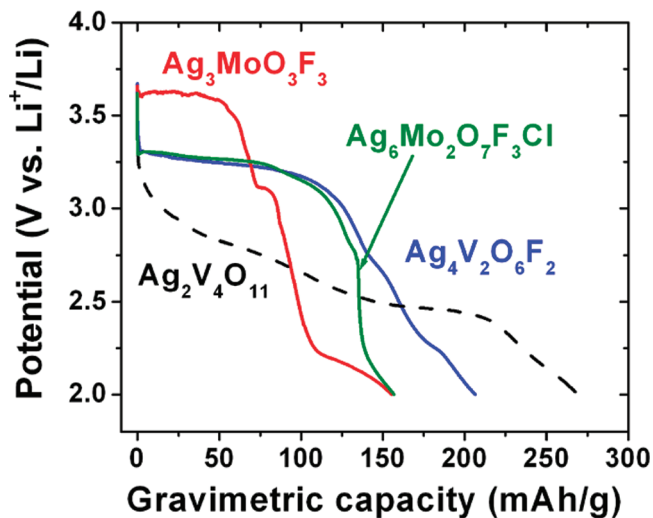


Figure 6. A comparison of the electrochemical discharge curves for $\text{Ag}_3\text{MoO}_3\text{F}_3$ (SMOF, red); $\text{Ag}_6\text{Mo}_2\text{O}_7\text{F}_3\text{Cl}$ (SMOFC, green); $\text{Ag}_4\text{V}_2\text{O}_6\text{F}_2$ (SVOF, blue); and $\text{Ag}_2\text{V}_4\text{O}_{11}$ (SVO, black) shows the higher potential of $\text{Ag}_3\text{MoO}_3\text{F}_3$ up to 70 mAh/g, and lower potential above 3 V. All samples were prepared hydrothermally at 150 °C and tested as cathode material in a Li battery test cell with a 13% weight carbon composite electrode at a discharge rate of 1 Li^+ in 10 h.

a displacement reaction.⁵ This step involves the reaction of approximately one lithium per formula unit and induces the collapse of the initial structure owing to the ionic radii mismatch between Ag^+ and Li^+ .^{1,5} In the second discharge region, between $1 \text{ Li}^+ < x < 2 \text{ Li}^+$, the voltage drops rapidly to 2.2 V before stabilizing close to 2 V, leading to the insertion of 2.8 Li^+ . This feature of rapid potential decline is relatively similar to recent observations with $\text{Ag}_6\text{Mo}_2\text{O}_7\text{F}_3\text{Cl}$, which begins to show reduction of Mo^{6+} in this area of the discharge curve.¹⁰ Tong et al. have reported the synthesis of $\text{Ag}_3\text{MoO}_3\text{F}_3$ by a mechanochemical procedure that leads to a more efficient lithium/silver displacement reaction.⁵ This discrepancy could be the result of the larger particle size in our study, which impedes the kinetics of the silver displacement reaction. In the case of $\text{Ag}_3\text{MoO}_3\text{F}_3$, this reaction is irreversible.

Although $\text{Ag}_3\text{VO}_2\text{F}_4$ adopts a structure similar to $\text{Ag}_3\text{MoO}_3\text{F}_3$, its reactivity vs lithium is significantly different; since only 0.3 Li^+ can be inserted above 2 V, $\text{Ag}_3\text{VO}_2\text{F}_4$ can be qualified as an inactive material. The cause of this unexpected lack of reactivity vs lithium is not yet completely understood; however, we speculate that a possible exchange reaction between silver and lithium within the electrolyte may occur. This is supported by the detection of silver metal at the surface of the lithium after the cell discharge. The electrochemical difference between these two cryolite type materials highlights the important role of the transition metal on the silver displacement reaction.

Figure 6 compares the discharge curves of $\text{Ag}_2\text{V}_4\text{O}_{11}$ (SVO), $\text{Ag}_4\text{V}_2\text{O}_6\text{F}_2$ (SVOF), $\text{Ag}_6\text{Mo}_2\text{O}_7\text{F}_3\text{Cl}$ (SMOFC), and $\text{Ag}_3\text{MoO}_3\text{F}_3$ (SMOF) under similar test conditions. The comparison highlights a clear advantage in the cryolite type structure for power delivery, seen as a noticeably higher potential for silver reduction. This primarily results from the lower overpotential for the silver extrusion in $\text{Ag}_3\text{MoO}_3\text{F}_3$.

Conclusions

The discovery of $\text{Ag}_3\text{MoO}_3\text{F}_3$ and $\text{Ag}_3\text{VO}_2\text{F}_4$ demonstrating a negative temperature coefficient of solubility allowed for the

synthesis and study of single crystals of both compounds. This precipitation by a heating technique may be useful for growing crystals in related chemical systems. Currently, these single crystalline products allow for a detailed determination of the structure, as well as examination of oxide and fluoride local order in these two recently reported cryolite type compounds.

Acknowledgment. The authors thank Professor Jean-Marie Tarascon for hosting F.S. to perform the electrochemical measurements, and Dr. Sylvie Malo and Dr. Amy Sarjeant for fruitful discussions. The authors gratefully acknowledge the support from the National Science Foundation (Solid State Chemistry Awards No. DMR-0604454), and the Office of Naval Research (MURI Grant N00014-07-1-0620). This work made use of the J. B. Cohen X-ray Diffraction Facility supported by the MRSEC program of the National Science Foundation (DMR-0520513) at the Materials Research Center of Northwestern University.

Supporting Information Available: A video of $\text{Ag}_3\text{VO}_2\text{F}_4$ single crystal growth at 90x speed (AVI); X-ray crystallographic files in CIF format for $\text{Ag}_3\text{MoO}_3\text{F}_3$ and $\text{Ag}_3\text{VO}_2\text{F}_4$, including crystallographic details, atomic coordinates, anisotropic thermal parameters, interatomic distances, and angles; and a precession figure showing modulation in $\text{Ag}_3\text{MoO}_3\text{F}_3$. This material is available free of charge via the Internet at <http://pubs.acs.org>.

References

- (1) Sauvage, F.; Bodenez, V.; Vezin, H.; Albrecht, T. A.; Tarascon, J.-M.; Poeppelmeier, K. R. *Inorg. Chem.* **2008**, *47*, 8464–8472.
- (2) Sorensen, E. M.; Izumi, H. K.; Vaughey, J. T.; Stern, C. L.; Poeppelmeier, K. R. *J. Am. Chem. Soc.* **2005**, *127*, 6347–6352.
- (3) Albrecht, T. A.; Sauvage, F.; Bodenez, V.; Tarascon, J.-M.; Poeppelmeier, K. R. *Chem. Mater.* **2009**, *21*, 3017–3020.
- (4) Yacoubi, A.; Grannec, J.; Tressaud, A.; Linke, D. *Mater. Lett.* **1989**, *7*, 385–390.
- (5) Tong, W.; Yoon, W.-S.; Hagh, N.; Amatucci, G. *Chem. Mater.* **2009**, *21*, 2139–2148.
- (6) Tong, W.; Amatucci, G. *Electrochem. Solid State* **2009**, *12*, A219–A224.
- (7) Albrecht, T. A.; Stern, C. L.; Poeppelmeier, K. R. *Inorg. Chem.* **2007**, *46*, 1704–1708.
- (8) Maggard, P. A.; Nault, T. S.; Stern, C. L.; Poeppelmeier, K. R. *J. Solid State Chem.* **2003**, *175*, 27–33.
- (9) Poeppelmeier, K. R.; Sauvage, F.; Bodenez, V.; Tarascon, J.-M. U.S. Provisional Patent 60/934160, 2007.
- (10) Sauvage, F.; Bodenez, V.; Tarascon, J.-M.; Poeppelmeier, K. R. *Inorg. Chem.* **2010**, *49*, 6461–6467.
- (11) Bertolini, J. C. *J. Emerg. Med.* **1992**, *10*, 163–168.
- (12) Peters, D.; Miethchen, R. *J. Fluorine Chem.* **1996**, *79*, 161–165.
- (13) Segal, E. B. *Chem. Health Saf.* **2000**, *7*, 18–23.
- (14) Harrison, W. T. A.; Nenoff, T. M.; Gler, T. E.; Stucky, G. D. *Inorg. Chem.* **1993**, *32*, 2437–41.
- (15) Norquist, A. J.; Heier, K. R.; Stern, C. L.; Poeppelmeier, K. R. *Inorg. Chem.* **1998**, *37*, 6495–6501.
- (16) Bruker APEX2 suite (SAINT v.7.34A, XPREP v2008/2, SADABS v2008/1, SHELXTL 6.14), v2008.5-0; Bruker AXS, Inc.: Madison, WI, USA, 2008.
- (17) Sheldrick, G. M. *TWINABS*; University of Göttingen: Germany, 2007.
- (18) $\text{HF}_{(\text{aq})}$ denotes the aqueous reagent (48–50% HF by weight) and HF (no subscript) denotes molecules in solution, regardless of water, calculated for a 49% $\text{HF}_{(\text{aq})}$ reagent.
- (19) Guo, H.-X.; Liu, S.-X. *Chin. J. Struct. Chem.* **2005**, *24*, 1452–1456.
- (20) The $\text{Ag}_2\text{Mo}_2\text{O}_7$ phase reported here is the structure by Guo et al., made via hydrothermal techniques, and different from the structure of identical chemical formula made by solid state synthesis by Gatehouse and Leverett.
- (21) Gatehouse, B. M.; Leverett, P. *J. Chem. Soc. Dalton* **1976**, *14*, 1316–1320.
- (22) Bateman, L. A.; Ferneliuss, W. C. *J. Chem. Educ.* **1937**, *14*, 315.
- (23) Kolb, E. D.; Barnes, R. L.; Laudise, R. A.; Grenier, J. C. *J. Cryst. Growth* **1980**, *50*, 404–418.
- (24) Marchetti, G. *Z. Anorg. Chem.* **1895**, *10*, 66–73.
- (25) Schmitz-Dumont, O.; Opgenhoff, P. *Z. Anorg. Allg. Chem.* **1954**, *275*, 21–31.
- (26) Sheldrick, G. M. *Acta Crystallogr. A* **2008**, *64*, 112–122.
- (27) Marvel, M. R.; Pinlac, R. F.; Lesage, J.; Stern, C. L.; Poeppelmeier, K. R. *Z. Anorg. Allg. Chem.* **2009**, *635*, 869–877.
- (28) Sheldrick, G. M. *CELL-NOW*; University of Göttingen: Germany, 2003.
- (29) Brink, F. J.; Noren, L.; Goossens, D. J.; Withers, R. L.; Jiu, Y.; Xu, C.-N. *J. Solid State Chem.* **2003**, *174*, 450–458.
- (30) Takeuchi, E. S.; Thiebolt, W. C., III. *J. Electrochem. Soc.* **1988**, *135*, 2691–2694.
- (31) Sauvage, F.; Bodenez, V.; Tarascon, J.-M.; Poeppelmeier, K. R. *J. Am. Chem. Soc.* **2010**, *132*, 6778–6782.